



## EFFECT OF STRESS AND LOAD DISTRIBUTION ANALYSIS ON AN ISOTROPIC RECTANGULAR PLATE

F. C. Onyeka

Department of Civil Engineering, Edo State University, Iyamho, Edo State, Nigeria

\*Corresponding author's email address: [onyeka.festus@edouniversity.edu.ng](mailto:onyeka.festus@edouniversity.edu.ng)

### ARTICLE INFORMATION

Submitted 5 February, 2020  
Revised 13 August, 2020  
Accepted 24 August, 2020

### Keywords:

static bending analysis  
CSFS rectangular plates  
shear deformation plate theory  
direct variation  
critical lateral imposed load

### ABSTRACT

Structural failure is discovered to be attributed to the inability of the designer to determine the structural load (critical load) that causes it. The aim of this study is to develop a mathematical model for calculation of the critical lateral imposed load of the plate before deflection reaches the maximum specified limit  $Q_{iw}$  and its corresponding critical lateral imposed load before plate reaches an elastic yield point  $Q_{ip}$ . Total potential energy equation of a thick plate was formulated from the static elastic theory of the plate. Direct variation method of analysis was adopted by minimizing the total potential energy obtained to determine the expression for the deflection and shear deformation. By solving the formulated expression, the effect of stress and load distribution analysis of a mild steel rectangular plate with one edge clamped, free at the other and the other opposite edge simply supported (CSFS) are analyzed and discussed. From the established equation, a new model for determination of the critical lateral imposed load of the plate is developed. The result showed that: (i) as the specified thickness of the plate increases, the value of critical lateral imposed load increase (ii) the critical lateral imposed load decrease as the plates span increases. (iii) the critical lateral imposed load increase as the plate thickness increases. (iv) increase in the value of the allowable deflection value required for the analysis of the plate reduces the chances of failure of a structural member. It is concluded that the values of critical lateral load obtained by this theory achieve accepted vertical shear stress to the thickness of plate variation and satisfied the transverse flexibility of the condition of the plate while predicting the flexural characteristics for an isotropic rectangular CSFS plate. Numerical comparison was conducted to verify and demonstrate the efficiency of the present theory. The results obtained are in good agreement with those in the literature. This approach is recommended to the practicing engineers as it overcomes the challenges of the conventional practice in the structural analysis/design which involves checking of deflection and shear; the process which is proved unreliable

© 2021 Faculty of Engineering, University of Maiduguri, Nigeria. All rights reserved.

### 1.0 Introduction

The important of plate structures in aerospace, aeronautic, automotive, military and structural engineering cannot be overemphasized. In structural engineering, they can be used as bridge deck, retaining wall for water retaining structures, panel for building slab, ship hull and spacecraft. Isotropic plates refer to plates whose material properties in all directions at a point are same while anisotropic or orthotropic plates refer to plates whose material properties are direction dependent. Isotropic thick plates are being widely used in structures subjected to uniformly distributed load, which produce a very large stresses on it (Gwarah, 2019 and Onyeka et al., 2020). To analyze the bending due to the applied load, the value of the critical load which efficiently causes the plate structure to be unstable as per equilibrium should be developed and evaluated. Critical Load is defined as the highest loading value, which will not cause any lateral deflection or tangential deflection on the structure (Onyeka et al., 2020). When the critical load exceeds the design load of the structure, it will be in deflecting position

(Onyeka, 2019). As the load is increased beyond the critical load the lateral deflections increase, until it may fail in other modes such as yielding of the material (Onyeka and Ibearugbulem, 2020). To avoid failure happening within the structural member, analytical approach to bending behavior is necessary to determine the critical load in the structure.

Since the classical plate theory (CPT) (Kirchhoff, 1850a; Kirchhoff, 1850b), which did not account for transverse shear effects proved unsatisfactory when applied to the isotropic plate analysis with large shear stress, shear deformation theory is obligatory.

Many shear deformation theories developed by many researchers (Ghugal, and Sayyad, 2011., Mantari et al., 2012., Mindlin, 1951., Ghugal et al., 2011., Reddy, 1984., Sayyad and Ghugal, 2012 a, b) considers the effect of shear deformation (TSDT, HSDT and ESDT respectively) to predict the bending and free vibration behavior of thick isotropic plates under uniformly distributed lateral load. Ghugal et al. (2011) applied the trigonometric shear deformation theory (TSDT) for the analysis of rectangular plates. Their theory and others (Pagno, 1967; Pipes and Pagano, 1970; Ghugal, and Sayyad, 2011; Mantari et al., 2012) incorporates the effect of transverse shear stress and shear deformation in the analysis. Results obtained using the above theory shows slight errors in predicting responses of the lateral load on the structures.

Polynomial displacement functions (Onyeka and Ibearugbulem, 2020) can be applied successfully to solve various boundary condition of thick rectangular plate; a feat that could not be easily achieved using trigonometric, hyperbolic and exponential shape functions. It will contribute in addressing the problem of dearth of literature on the function of polynomial displacement functions. Scholars and practicing engineers will assess, apply and sustain trust in their works/designs. Thereby the psychological trauma due to doubt or not too sure of ones works using Fourier series to analyze thick plates will be done away with.

Ibearugbulem and Onyeka, (2020) used the polynomial shear deformation theory (PSDT) for the analysis of rectangular plates. Their theory incorporates the effect of transverse shear stress and shear deformation in the analysis. Results obtained using the theories did not introduce much error in the analysis, but it ended up determining the displacements, moments and stresses that may occur due to the applied load without obtaining the critical lateral load in predicting responses of the applied load which can lead to failure on the structures.

Nonlinear strain–displacement polynomial shape function of third order shear deformation theory was used for rectangular thick plate analysis under uniformly distributed load (Onyeka and Ibearugbulem, 2020). They determine imposed load that causes deflection of rectangular plates with all four edges clamped (CCCC) and plate with free of support at third edge and the other edges clamped (CCFC) rectangular thick, but did not obtain for other type of plate.

In this work, the static bending analysis of an isotropic rectangular plate subjected to uniform distributed transverse loads was presented using displacement and refined shear deformation theory. This theory, which is based on traditional higher-order shear deformation was applied in a bending analysis of rectangular plate with one edge clamped, free at the other and the other opposite edge simply supported (CSFS) to determine the effect of stress and load distribution analysis on an isotropic rectangular plate.

## 2. Displacement and Constitutive Relations

The elastic plate under lateral loading as shown in Figure 1 was used to obtain the displacement – strain relationships in terms of curvatures.

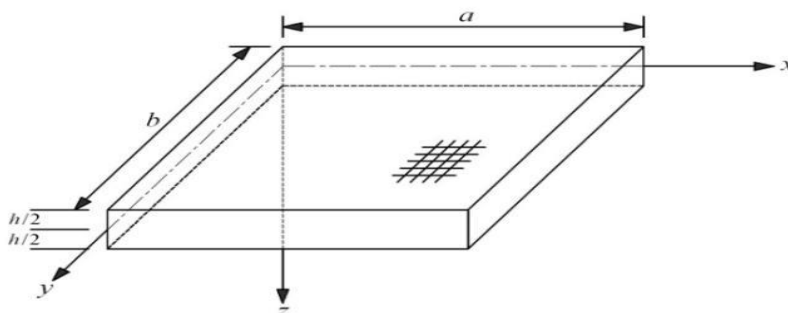


Figure 1: Rectangular plate under bending subjected to uniformly distributed load

The three displacement equations of thick plate assumed to be involved are: the deflection,  $w(x,y)$  and the two inplane displacements,  $u(x,y,z)$ , and  $v(x,y,z)$  were used to establish the constitutive equations of the rectangular plate.

The constitutive equations for five stress components (Onyeka et al., 2018) are:

$$\sigma_x = \frac{Ez}{1 - \mu^2} \left( \left( -\frac{d^2w}{dx^2} + \frac{Fd\theta_{Sx}}{dx} \right) + \mu \left( \frac{d^2w}{dy^2} + \frac{Fd\theta_{Sx}}{dy} \right) \right) \quad 1$$

$$\sigma_y = \frac{Ez}{1 - \mu^2} \left( \left( -\frac{d^2w}{dy^2} + \frac{Fd\theta_{Sx}}{dx} \right) + \mu \left( \frac{d^2w}{dx^2} + \frac{Fd\theta_{Sx}}{dy} \right) \right) \quad 2$$

Also, from known state Equation,

$$\tau_{xy} = \frac{E(1 - \mu)}{(1 - \mu^2)} \left( -\frac{z\partial^2w}{\partial x\partial y} + F \left( \frac{d\theta_{Sx}}{dy} + \frac{d\theta_{Sy}}{dx} \right) \right) \quad 3$$

Similarly,

$$\tau_{xz} = \frac{E(1 - \mu)}{(1 - \mu^2)} \left( \frac{z\partial^2w}{\partial x\partial z} + F \left( \frac{d\theta_{Sx}}{dz} + \frac{d\theta_{Sz}}{dx} \right) \right) \quad 4$$

Also,

$$\tau_{yz} = \frac{E(1 - \mu)}{(1 - \mu^2)} \left( \frac{z\partial^2w}{\partial y\partial z} + F \left( \frac{d\theta_{Sy}}{dz} + \frac{d\theta_{Sz}}{dy} \right) \right) \quad 5$$

$$\therefore \sigma_x = \frac{E(\epsilon_x + \mu\epsilon_y)}{1 - \mu^2} \quad 6$$

Similarly reasoning in y direction, we obtain:

$$\sigma_y = \frac{E(\epsilon_y + \mu\epsilon_x)}{1 - \mu^2} \quad 7$$

Similarly reasoning in z direction, we obtain:

$$\sigma_z = \frac{E(\epsilon_z + \mu\epsilon_x)}{1 - \mu^2} \quad 8$$

Similarly;

$$\tau_{xy} = \frac{E}{2(1 + \mu)} \cdot \gamma_{xy} \quad 9$$

$$\tau_{xz} = \frac{E}{2(1 + \mu)} \cdot \gamma_{xz} \quad 10$$

$$\tau_{yz} = \frac{E}{2(1 + \mu)} \cdot \gamma_{yz} \quad 11$$

### 3. Direct Governing Energy Equation

The direct variational method is used to obtain the direct governing differential equation by differentiating the total potential energy with respect to the coefficient of deflection  $A_s$ , coefficient of shear deformation with respect to x-axis  $A_x$  and coefficient of shear deformation with respect to y-axis  $A_y$ .

The total potential energy functional ( $\Pi$ ), the deflection and in – plane displacement functions ( $w, v$  and  $u$ ) of thick isotropic plate were derived (Onyeka et al., 2018), as:

$$\Pi = U + V \quad 12$$

where:

$$V = - \int_0^a \int_0^b q w(x, y) \partial x \partial y \quad 13$$

Therefore:

$$\begin{aligned} \Pi &= \frac{D}{2} \int_0^a \int_0^b \left[ \left| g_1 \left( \frac{\partial^2 w}{\partial x^2} \right)^2 - 2g_2 \left( \frac{\partial^2 w}{\partial x^2} \cdot \frac{\partial \theta_{Sx}}{\partial x} \right) + g_3 \left( \frac{\partial \theta_{Sx}}{\partial x} \right)^2 \right| \right. \\ &+ \left| 2g_1 \left( \frac{\partial^2 w}{\partial x \partial y} \right)^2 - 2g_2 \left( \frac{\partial^2 w}{\partial x \partial y} \cdot \frac{\partial \theta_{Sx}}{\partial y} \right) - 2g_2 \left( \frac{\partial^2 w}{\partial x \partial y} \cdot \frac{\partial \theta_{Sy}}{\partial x} \right) \right| + \left| (1 + \mu) g_3 \left( \frac{\partial \theta_{Sx}}{\partial y} \right) \left( \frac{\partial \theta_{Sy}}{\partial x} \right) \right| \\ &+ \frac{(1 - \mu)}{2} \left| g_3 \left( \frac{\partial \theta_{Sx}}{\partial y} \right)^2 + g_3 \left( \frac{\partial \theta_{Sy}}{\partial x} \right)^2 \right| + \left| g_1 \left( \frac{\partial^2 w}{\partial y^2} \right)^2 - 2g_2 \left( \frac{\partial^2 w}{\partial y^2} \cdot \frac{\partial \theta_{Sy}}{\partial y} \right) + g_3 \left( \frac{\partial \theta_{Sy}}{\partial y} \right)^2 \right| \\ &+ \left. \left| \frac{(1 - \mu)}{2} g_4 (\theta_{Sx})^2 + \frac{(1 - \mu)}{2} g_4 (\theta_{Sy})^2 \right| \right] \partial x \partial y \\ &- \int_0^a \int_0^b q w(x, y) \partial x \partial y \quad 14 \end{aligned}$$

Let:

$$w = A_s \cdot h \quad 15$$

$$\theta_{Sx} = \theta_{Sxx} \cdot \theta_{Sxy} = \left[ \frac{dh}{dR} \right] [A_x] \quad 16$$

And;

$$\theta_{Sy} = \theta_{Syy} \cdot \theta_{Syy} = \left[ \frac{dh}{dQ} \right] [A_y] \quad 17$$

$$\frac{\partial \Pi}{\partial A_1} = \frac{\partial \Pi}{\partial A_2} = \frac{\partial \Pi}{\partial A_3} = 0 \quad 18$$

The solution of the three governing equations of equilibrium are summarized as:

$$\int_0^1 \int_0^1 \left[ A_1 g_1 \left( k_1 + \frac{2}{\alpha^2} k_2 + \frac{1}{\alpha^4} k_3 \right) - A_2 g_2 \left( k_1 + \frac{1}{\alpha^2} k_2 \right) - A_3 g_2 \left( \frac{1}{\alpha^2} k_2 + \frac{1}{\alpha^4} k_3 \right) \right] dRdQ$$

$$= \frac{qa^4}{D} \int_0^1 \int_0^1 k_6 \cdot dRdQ \quad 19$$

$$\int_0^1 \int_0^1 \left[ -A_1 g_2 \left( k_1 + \frac{1}{\alpha^2} k_2 \right) + A_2 \left( g_3 k_1 + \frac{(1-\mu)}{2 \alpha^2} g_3 k_2 + \frac{(1-\mu)}{2} \rho^2 g_4 k_4 \right) \right. \\ \left. + A_3 \frac{(1+\mu)}{2 \alpha^2} g_3 k_2 \right] dRdQ = 0 \quad 20$$

$$\int_0^1 \int_0^1 \left[ -A_1 g_2 \left( \frac{1}{\alpha^2} k_2 + \frac{1}{\alpha^4} k_3 \right) + A_2 g_3 \frac{(1+\mu)}{2 \alpha^2} k_2 + A_3 g_3 \frac{(1-\mu)}{2} \left( \frac{1}{\alpha^2} k_2 + \frac{1}{\alpha^4} k_3 \right) \right. \\ \left. + A_3 g_4 \frac{(1-\mu)}{2 \alpha^2} \rho^2 k_5 \right] dRdQ = 0 \quad 21$$

Let:

$$r_{11} = g_1 \left( k_1 + \frac{2}{\alpha^2} k_2 + \frac{1}{\alpha^4} k_3 \right) \quad 22$$

$$r_{12} = -g_2 \left( k_1 + \frac{1}{\alpha^2} k_2 \right) \quad 23$$

$$r_{13} = -g_2 \left( \frac{1}{\alpha^2} k_2 + \frac{1}{\alpha^4} k_3 \right) \quad 24$$

$$r_{21} = -g_2 \left( k_1 + \frac{1}{\alpha^2} k_2 \right) \quad 25$$

$$r_{22} = \left( g_3 k_1 + \frac{(1-\mu)}{2 \alpha^2} g_3 k_2 + \frac{(1-\mu)}{2} \rho^2 g_4 k_4 \right) \quad 26$$

$$r_{23} = g_3 \frac{(1+\mu)}{2 \alpha^2} k_2 \quad 27$$

$$r_{31} = -g_2 \left( \frac{1}{\alpha^2} k_2 + \frac{1}{\alpha^4} k_3 \right) \quad 28$$

$$r_{32} = g_3 \frac{(1+\mu)}{2 \alpha^2} k_2 \quad 29$$

$$r_{33} = \left( g_3 \frac{(1-\mu)}{2} \left( \frac{1}{\alpha^2} k_2 + \frac{1}{\alpha^4} k_3 \right) + g_4 \frac{(1-\mu)}{2 \alpha^2} \rho^2 k_5 \right) \quad 30$$

and;

$$k_1 = \int_0^1 \int_0^1 \left( \frac{d^2 h}{dR^2} \right)^2 dRdQ \quad 31$$

$$k_2 = \int_0^1 \int_0^1 \left( \frac{d^2 h}{dRdQ} \right)^2 dRdQ \quad 32$$

$$k_3 = \int_0^1 \int_0^1 \left( \frac{d^2 h}{dQ^2} \right)^2 dRdQ \quad 33$$

$$k_4 = \int_0^1 \int_0^1 \left(\frac{dh}{dR}\right)^2 dRdQ \quad 34$$

$$k_5 = \int_0^1 \int_0^1 \left(\frac{dh}{dQ}\right)^2 dRdQ \quad 35$$

$$k_q = \int_0^1 \int_0^1 h. dRdQ \quad 36$$

where:

$$T_2 = \frac{r_{21} \cdot r_{33} - r_{23} \cdot r_{31}}{r_{22} \cdot r_{33} - r_{23} \cdot r_{32}} \quad 37$$

$$T_3 = \frac{r_{21} \cdot r_{32} - r_{22} \cdot r_{31}}{r_{23} \cdot r_{32} - r_{22} \cdot r_{33}} \quad 38$$

$$T_1 = 1 \quad 39$$

Thus:

$$A_s = \frac{qa^4}{D} \left( \frac{k_q}{r_{11}T_1 - r_{12}T_2 - r_{13}T_3} \right) \quad 40$$

where:

$A_s$  = Coefficient of deflection

#### 4.0 Formulation of the Critical Lateral Imposed Load in the Rectangular Plate

The formulae for calculating the critical imposed load before deflection reaches specified maximum limit,  $q_w$  and its corresponding critical lateral imposed load of the plate before plate reaches an elastic yield stress,  $q_x$  is developed using equation established from the previous sections.

To ensure that the critical lateral load the plate is determined before it reaches yielding, (Onyeka and Ibearugbulem, 2020):

$$w = A_s h < w_a \quad 41$$

$$\frac{12(1 - \mu^2)qa^4}{Et^3} \cdot \left( \frac{k_q}{r_{11} - r_{12}T_2 - r_{13}T_3} \right) \cdot h < w_a \quad 42$$

where,

$w_a$  = Allowable deflection

Also,

$$q = w_s + q_w \quad 43$$

This gives:

$$q_w < Et^3 \frac{w_a (r_{11} - r_{12}T_2 - r_{13}T_3)}{(1 - \mu^2)12 \cdot k_q \cdot ha^4} - \gamma \quad 44$$

where;

$w_s$  = Self weight of the plate

And,

$q_w$  = Critical Imposed load of the plate before deflection reaches elastic limit

Also, to ensure that the critical lateral load the plate is determined before it reaches yielding; recall that:

$$U = \frac{1}{2} \iiint_{-\frac{t}{2}}^{\frac{t}{2}} \cap dx dy dz \quad 45$$

where;

$$\cap = \sigma_x \varepsilon_x + \sigma_y \varepsilon_y + \tau_{xy} \gamma_{xy} + \tau_{xz} \gamma_{xz} + \tau_{yz} \gamma_{yz} \quad 46$$

Therefore:

$$\cap = \frac{1}{E} [\sigma_x^2 - \mu \sigma_x \sigma_y - \mu \sigma_x \sigma_y + \sigma_y^2 + 2(1 + \mu) \tau_{xy}^2 + 2(1 + \mu) \tau_{xz}^2 + 2(1 + \mu) \tau_{yz}^2] \quad 47$$

This gives:

$$\cap = \frac{1}{E} [\sigma_x^2 - \mu \sigma_x \sigma_y - \mu \sigma_x \sigma_y + \sigma_y^2 + 2(1 + \mu) \tau_{xy}^2 + 2(1 + \mu) \tau_{xz}^2 + 2(1 + \mu) \tau_{yz}^2] < \cap_0 \quad 48$$

Let:

$$\varepsilon_x = \frac{\sigma_x - \mu \sigma_y}{E} \quad 49$$

$$\varepsilon_y = \frac{\sigma_y - \mu \sigma_x}{E} \quad 50$$

$$\gamma_{xy} = \frac{2(1 + \mu) \tau_{xy}}{E} \quad 51$$

Similarly,

$$\gamma_{xz} = \frac{2(1 + \mu) \tau_{xz}}{E} \quad 52$$

Also,

$$\gamma_{yz} = \frac{2(1 + \mu) \tau_{yz}}{E} \quad 53$$

$\cap_0$  = yielding point of the plate.

For a bar,

$$\text{let } \sigma_x = fy \text{ and } \sigma_y = \tau_{xy} = \tau_{xz} = \tau_{yz} = 0 \quad 54$$

Therefore;

$$\cap < \cap_0 > \frac{fy^2}{E} \quad 55$$

Putting Equation 48 into 55; we have:

$$\frac{1}{E} [\sigma_x^2 - 2\mu \sigma_x \sigma_y + \sigma_y^2 + 2(1 + \mu) \tau_{xy}^2 + 2(1 + \mu) \tau_{xz}^2 + 2(1 + \mu) \tau_{yz}^2] < \frac{fy^2}{E} \quad 56$$

Let,

$$\sigma_y = n_1 \sigma_x \quad 57$$

$$\tau_{xy} = n_2 \sigma_x \quad 58$$

$$\tau_{xz} = n_3 \sigma_x \quad 59$$

$$\tau_{yz} = n_4 \sigma_x \quad 60$$

Therefore, substituting Equations 57, 58, 59 and 60 into 49, we have:

$$\sigma_x < \frac{fy}{[1 - 2\mu n_1 + n_1^2 + 2(1 + \mu) n_2^2 + 2(1 + \mu) n_3^2 + 2(1 + \mu) n_4^2]} \quad 61$$

By simplifying equation 1 and 6, the value of  $\sigma_x$  becomes;

$$\sigma_x = \frac{12. q a^2}{t^3} \cdot \frac{k_q}{k_T} z \left( \frac{d^2 h}{dR^2} + \frac{\mu}{\alpha^2} \frac{d^2 h}{dQ^2} \right) \quad 62$$

By equating Equation 61 and 62, we have:

$$\frac{12. qa^2. k_q}{k_T t^3} \cdot z \phi_2 < \frac{fy}{\phi_3} \quad 63$$

This gives:

$$\sigma_x < \frac{fy}{\phi_3} \quad 64$$

This gave:

$$\sigma_x = \frac{qa^4 Ez \phi_2}{(1 - \mu^2) D \alpha^2} \cdot \left( \frac{k_q}{r_{11} T_1 - r_{12} T_2 - r_{13} T_3} \right) \quad 65$$

Recall,

$$A_1 = \frac{qa^4}{D} \left( \frac{k_q}{r_{11} T_1 - r_{12} T_2 - r_{13} T_3} \right) \quad 66$$

Let;

$$D = \frac{Et^3}{12(1 - \mu^2)} \quad 67$$

where;

$$\phi_2 = \left( \frac{d^2 h}{dR^2} + \frac{\mu}{\alpha^2} \frac{d^2 h}{dQ^2} \right) \quad 68$$

and,

$$\phi_3 = \sqrt{[1 - 2\mu n_1 + n_1^2 + 2(1 + \mu)n_2^2 + 2(1 + \mu)n_3^2 + 2(1 + \mu)n_4^2]} \quad 69$$

From Equation 63, we got expression for q as:

$$q < \frac{fy t^3}{12. a^2. k. z. \phi_2. \phi_3} \quad 70$$

Let;

$$q = w_s + q_x \quad 71$$

This gives:

$$q_x < \frac{fy t^3}{12. a^2. \frac{k_q}{k_T} \cdot z. \phi_2. \phi_3} - w_s \quad 72$$

This gave:

$$q_x < \frac{k_T fy t^3}{12. a^2. k_q \cdot z. \phi_2 \phi_3} - w_s \quad 73$$

$q_x$  = critical imposed lateral load before plate reach elastic yield stress

$fy$  = characteristic strength of the steel plate

and;

$w_s$  = self weight of the plate

$t$  = specific thickness of the plate

## 5. Numerical Problem

The particular shape function for rectangular plate with their respective boundary is shown in Figure 2.

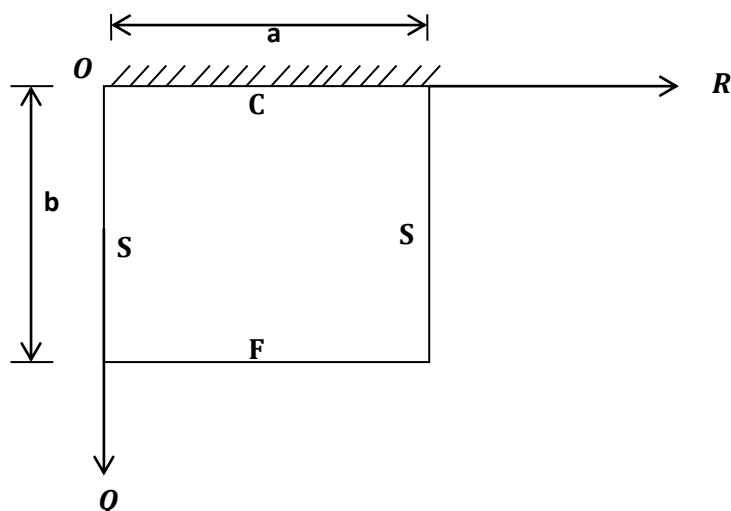


Figure 2: CSFS Rectangular Plate

Considering the Figure 2, the numerical analysis of CSFS rectangular plate of various span-thickness ratios are presented in Figure 4 to 12.

A polynomial shear deformation function was applied to the governing equation obtained in the previous section to determine the numerical values of stiffness coefficients in Equation 31 to 36.

The fourth order polynomial displacement function for the analysis CSFS plate was derived as presented in Equation 74:

$$w = (F_{a4} \cdot b_5) \left[ (R^2 - 2R^3 + R^4) \times \left( \frac{7Q}{3} - \frac{10}{3}Q^3 + \frac{10}{3}Q^4 - Q^5 \right) \right] / 8640 \quad 74$$

Let the amplitude,

$$A_s = \frac{(F_{a4} \times F_{b4})}{8640} \quad 75$$

And shape function;

$$h = (R^2 - 2R^3 + R^4) \times \left( \frac{7Q}{3} - \frac{10}{3}Q^3 + \frac{10}{3}Q^4 - Q^5 \right) \quad 76$$

## 6. Results and Discussion

The values stiffness coefficient obtained from Equation 31 to 36 is presented in Table I. These values when substituted appropriately aid the solution for the coefficients of deflection, shear deformation and stresses in the plate.

Table I: Values of Stiffness Coefficient, k for Various Support (boundary conditions)

PLATE	$k_1$	$k_2$	$k_3$	$k_4$	$k_5$	$k_q$
CSFS	0.3284779	0.0919002	0.1286676	0.0332388	0.00931015	0.0453

From the numerical analysis obtained as presented in the Figures 4 to 12, it is if found that as the specified thickness (t) of plate increases, the value of critical lateral imposed load  $q_w$  and  $q_x$  increases. This implies that as we increase the thickness of the plate safety is ensured in the plate structure.

Figures 4 to 12 presents the result of CSFS plate with span of 1000mm, 3000mm and 5000mm at allowable deflection of 1mm, 3mm and 5mm at 5mm, 7.5mm, 10mm, 12.5mm and 15mm specified thickness. From the result, the value of  $q_w$  and  $q_x$  is between -1.1446 N/mm to 53.413 N/mm and -0.1335 N/mm to 68.517 N/mm been the highest and lowest value at respectively. From the table, it is seen that the values of critical lateral imposed load  $q_w$  and  $q_x$  decrease as the length-width ratio increases, this continues until failure occurs. This showed that the greatest failure (at -1.1446 N/mm) occurs at span to breadth ratio and allowable thickness of 2 and 15mm respectively. This means that an increase in plate length increases the chance of failure in a plate structure.

From the numerical analysis obtained as presented in the Figure 4 to 12, it finds that as the specified thickness (t) of plate increases, the value of critical lateral imposed load  $q_w$  and  $q_x$  increases. This implies that, increase in the thickness of the plate ensured safety in the plate structure.

Figures 4 to 12 presents the result of CSFS plate with span of 1000mm, 3000mm and 5000mm at allowable deflection of 1mm, 3mm and 5mm at 5mm, 7.5mm, 10mm, 12.5mm and 15mm specified thickness. From the result, the value of  $q_w$  and  $q_x$  is between -1.1446 N/mm to 53.413 N/mm and -0.1335 N/mm to 68.517 N/mm been the highest and lowest value at respectively. From the table, it is seen that the values of critical lateral imposed load  $q_w$  and  $q_x$  decrease as the length-width ratio increases, this continues until failure occurs. This showed that the greatest failure (at -1.1446 N/mm) occurs at span to breadth ratio and allowable thickness of 2 and 15mm respectively. This means that an increase in plate length increases the chance of failure in a plate structure.

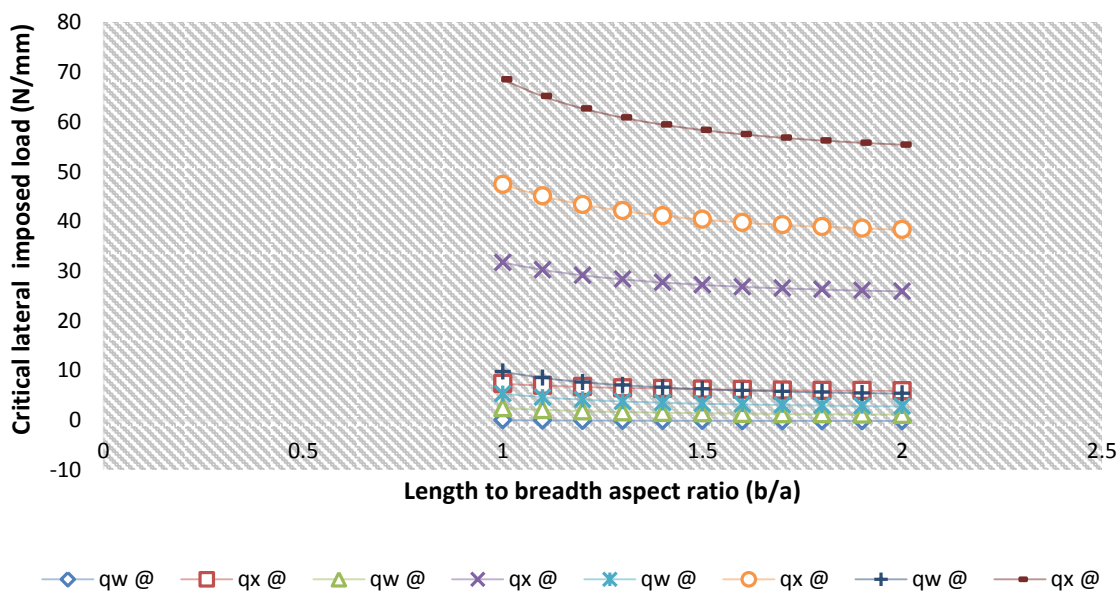


Figure 4: Plots of critical lateral imposed load versus length to breadth ratio of CSFS plate for span, a = 1000mm at  $w_a = 1.0$ mm

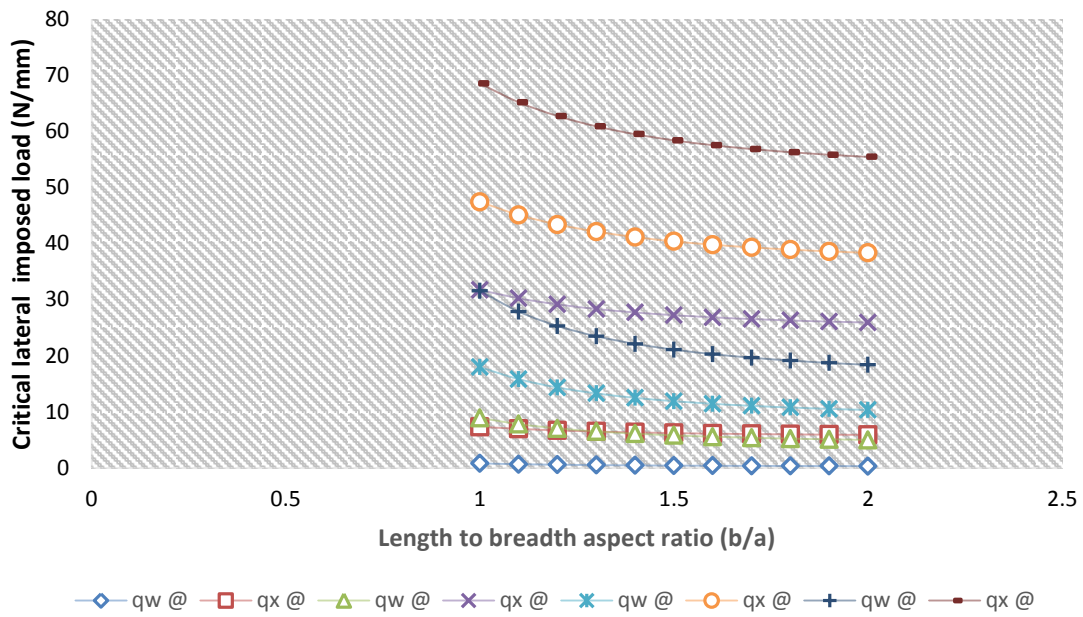


Figure 5: Plots of critical lateral imposed load versus length to breadth ratio of CSFS plate for span,  $a = 1000\text{mm}$  at  $w_a = 3.0\text{mm}$

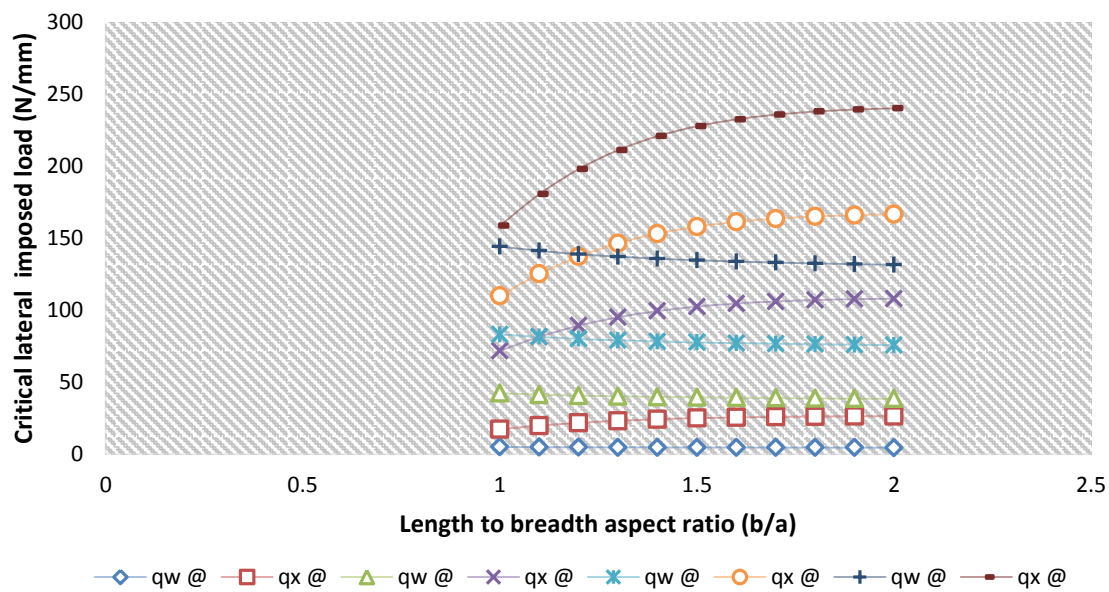


Figure 6: Plots of critical lateral imposed load versus length to breadth ratio of CSFS plate for span,  $a = 1000\text{mm}$  at  $w_a = 5.0\text{mm}$

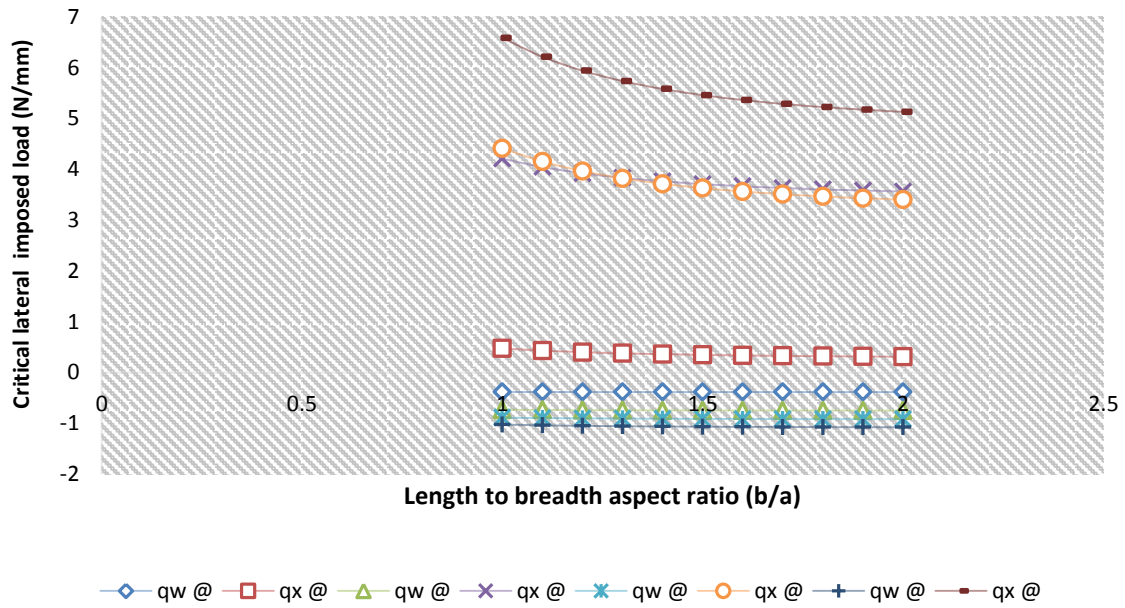


Figure 7: Plots of critical lateral imposed load versus length to breadth ratio of CSFS plate for span,  $a = 3000\text{mm}$  at  $w_a = 1.0\text{mm}$

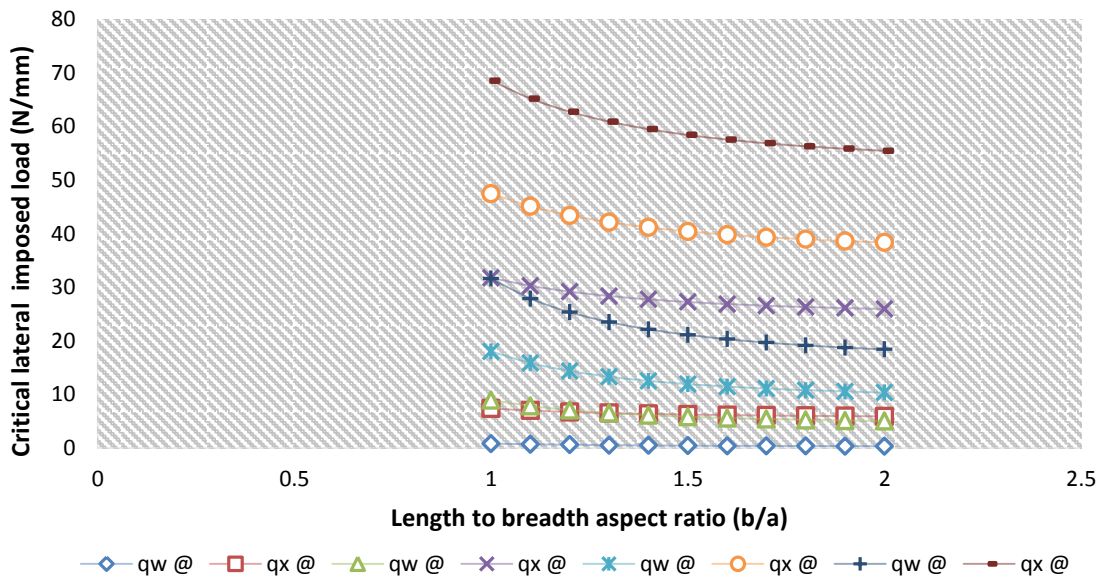


Figure 8: Plots of critical lateral imposed load versus length to breadth ratio of CSFS plate for span,  $a = 3000\text{mm}$  at  $w_a = 3.0\text{mm}$

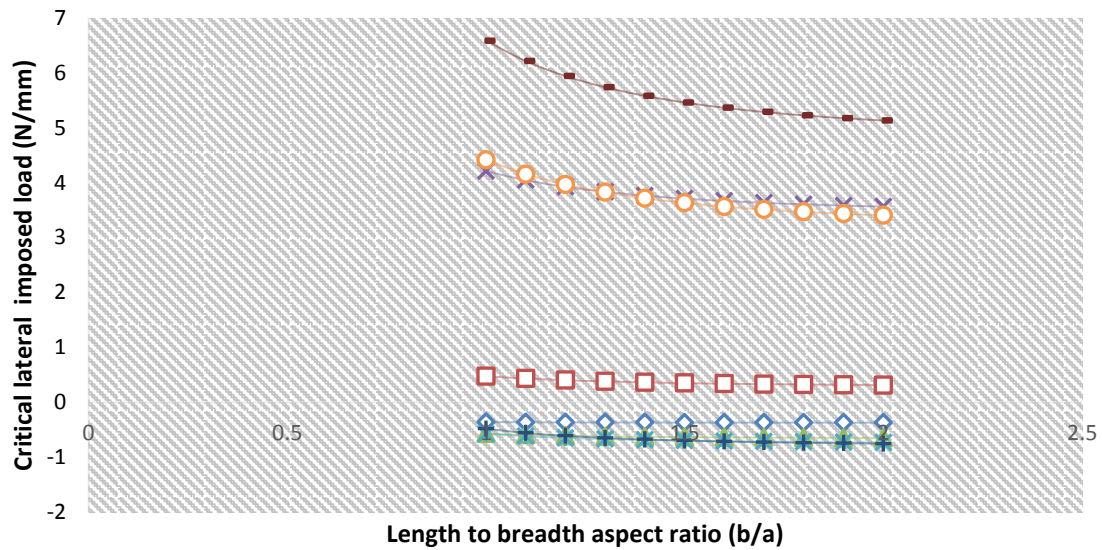


Figure 9: Plots of critical lateral imposed load versus length to breadth ratio of CSFS plate for span, a = 3000mm at w<sub>a</sub> = 5.0mm

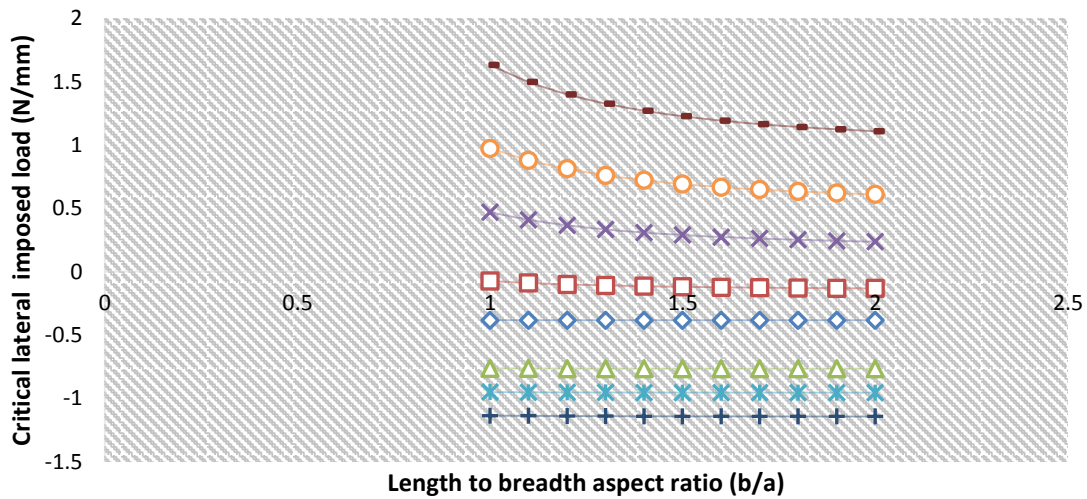


Figure 10: Plots of critical lateral imposed load versus length to breadth ratio of CSFS plate for span, a = 5000mm at w<sub>a</sub> = 1.0mm

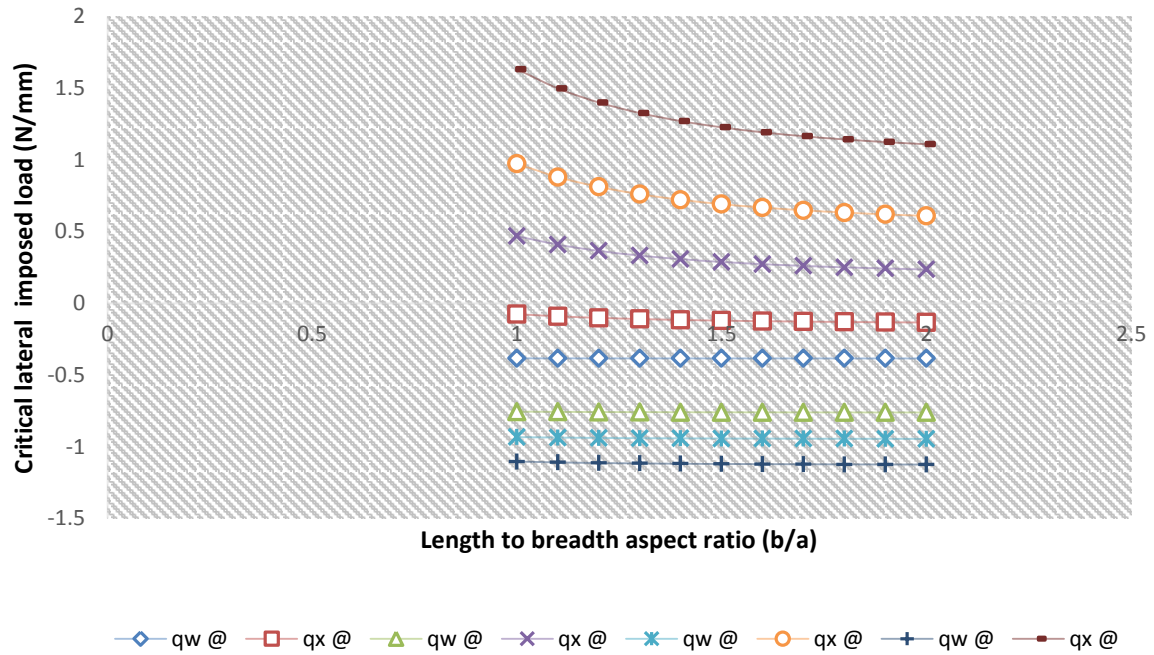


Figure 11: Plots of critical lateral imposed load versus length to breadth ratio of CSFS plate for span,  $a = 5000\text{mm}$  at  $w_a = 3.0\text{mm}$

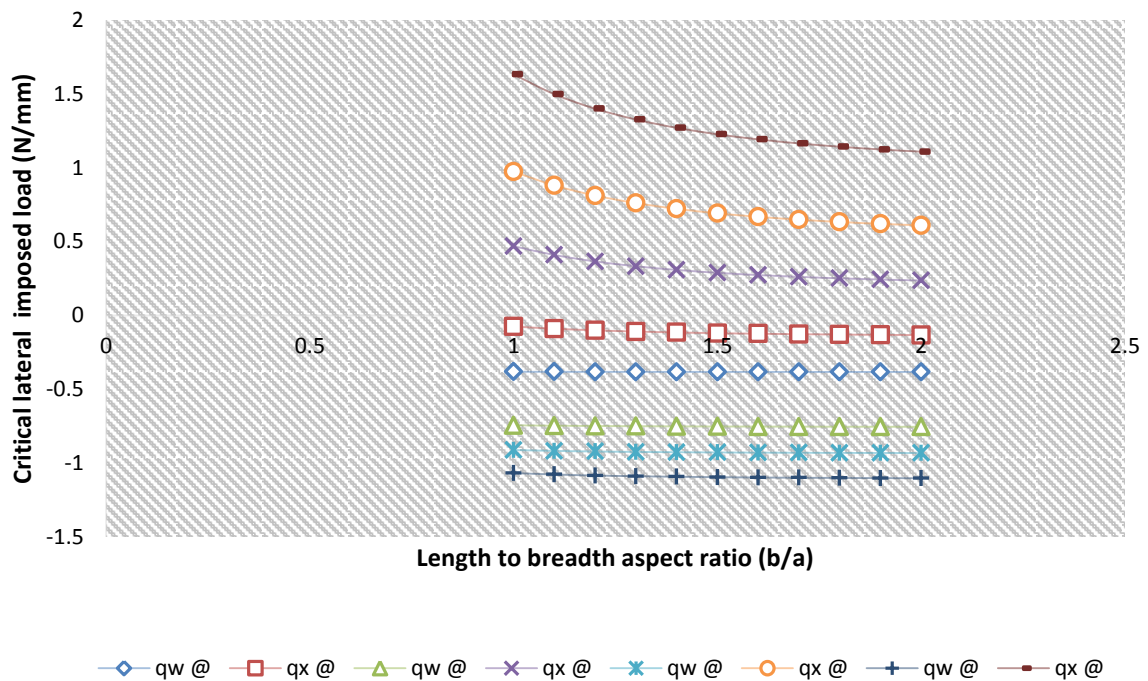


Figure 12: Plots of critical lateral imposed load versus length to breadth ratio of CSFS plate for span,  $a = 5000\text{mm}$  at  $w_a = 5.0\text{mm}$

Looking closely at Figures 5 to 7 (CSFS plate with span of 1000mm at allowable deflection ( $w_a$ ) value between 1mm to 5mm). It is found that failure of critical lateral imposed load ( $q_w$ ) only occur at a thickness of 5mm which is between the length to width ratio of 1.1, 1.2, 1.3, 1.4, 1.5, 1.6, 1.8, 1.9 and 2 with a value of -0.0266N/mm, -0.0582N/mm, 0.0808N/mm, -0.0976N/mm, -0.01103N/mm, -0.1202N/mm, -0.1280N/mm, -0.1343N/mm, -0.1395N/mm and -0.1438N/mm.

Looking closely at Figures 8 to 10 (CSFS plate with a span of 3000mm at allowable deflection ( $w_a$ ) value between 1mm to 5mm). It is found that failure of critical lateral imposed load ( $q_w$ ) only occur at a thickness of 1mm and 5mm which is between the length to width ratio of 1, 1.1, 1.2, 1.3, 1.4, 1.5, 1.6, 1.8, 1.9 and 2 for all specified thickness value. This shows that the value of critical lateral imposed load ( $q_w$ ), while the critical imposed load ( $q_x$ ) remains positive (safe). This means that an increase in the value of the specified deflection failure tendency of the plate structure.

The result of critical lateral imposed load for CSFS plate with span of 1000mm at allowable deflection ( $w_a$ ) of 1mm, 3mm and 5mm is presented in Figure 5 to 7. It finds that the failure of critical lateral imposed load ( $q_w$ ) only occur at a thickness of 5mm which is between the length to width ratio of 1.1, 1.2, 1.3, 1.4, 1.5, 1.6, 1.8, 1.9 and 2 with a value of -0.0266N/mm, -0.0582N/mm, 0.0808N/mm, -0.0976N/mm, -0.01103N/mm, -0.1202N/mm, -0.1280N/mm, -0.1343N/mm, -0.1395N/mm and -0.1438N/mm.

Furthermore, the result of critical lateral imposed load for CSFS plate with span of 3000mm at allowable deflection ( $w_a$ ) of 1mm, 3mm and 5mm is presented in Figure 8 to 10. It finds that the failure of critical lateral imposed load ( $q_w$ ) only occur at a thickness of 1mm and 5mm which is between the length to width ratio of 1, 1.1, 1.2, 1.3, 1.4, 1.5, 1.6, 1.8, 1.9 and 2 for all specified thickness value.

Looking closely at Figures 11 to 13 (CSFS plate with span of 5000mm at allowable deflection ( $w_a$ ) value between 1mm to 5mm). It is found that failure of critical lateral imposed load ( $q_w$  and  $q_x$ ) occur at specified thickness 5mm and 7.5mm which is between the length to width ratio of 1, 1.1, 1.2, 1.3, 1.4, 1.5, 1.6, 1.8, 1.9 and 2 for all allowable deflection value while critical lateral imposed load ( $q_w$ ) only occur at other thickness at all length to width ratio and allowable deflection. Finally, the result of critical lateral imposed load for CSFS plate with span of 5000mm at allowable deflection ( $w_a$ ) of 1mm, 3mm and 5mm is presented in Figures 11 to 13. It finds that the failure of critical lateral imposed load ( $q_w$  and  $q_x$ ) occur at specified thickness 5mm and 7.5mm which is between the length to width ratio of 1, 1.1, 1.2, 1.3, 1.4, 1.5, 1.6, 1.8, 1.9 and 2 for all allowable deflection value while critical lateral imposed load ( $q_w$ ) only occur at other thickness at all length to width ratio and allowable deflection. The negative value of critical lateral imposed load  $q_w$  (and positive value of ( $q_x$ )) only reveals that the plate fails in  $q_w$  for the entire plate  $w_a$  (1mm to 5mm) and span of 1000mm to 5000mm. This means that the plate structure is not safe and required maintenance. The negative value of critical lateral imposed load ( $q_w$  and  $q_x$ ) reveals that the plate fails in both ( $q_w$  and  $q_x$ ) for the entire plate  $w_a$  (1mm to 5mm) for all types of plate. This means the total failure plate structure and this lead to collapse.

Table 2: Percentage difference between the values of non-dimensional center deflection of CSFS square rectangular plates from present and past studies

$\rho = \frac{a}{t}$	Present work	Gwarah, (2019)	Percentage Difference
4	0.006637	0.007297	9.052763
5	0.006087	0.006715	9.351812
10	0.005372	0.005929	9.402254
20	0.005196	0.00573	9.331607
30	0.005163	0.005693	9.314134
40	0.005152	0.00568	9.307697
50	0.005146	0.005674	9.304658
60	0.005144	0.005671	9.302937
70	0.005142	0.005669	9.301919
80	0.005141	0.005668	9.301357
90	0.00514	0.005667	9.300861
100	0.005139	0.005666	9.300466
Average % Difference		9.3	9.297705
Total % Difference		9.3	

The result of the comparison made in Table 1, shows that the total average percentage difference between the present study and that of Gwarah (2019) is 9.3%. This reveals that the difference between the two values is very negligible. They present good interpretations of the result. Hence, the direct variational method can be used with confidence for analysis of deflection on a CSFS rectangular plate.

From the Figure 13, it can be seen that the results obtained in this work agree very well with those from the previous work (Gwarah, 2019). The disparity between the values in bending is clear but still in agreement with each other. Hence, the approximating function according to polynomial function can be used reliably for analysis of a plate with one edge clamped, free at the other and the other opposite edge simply supported.

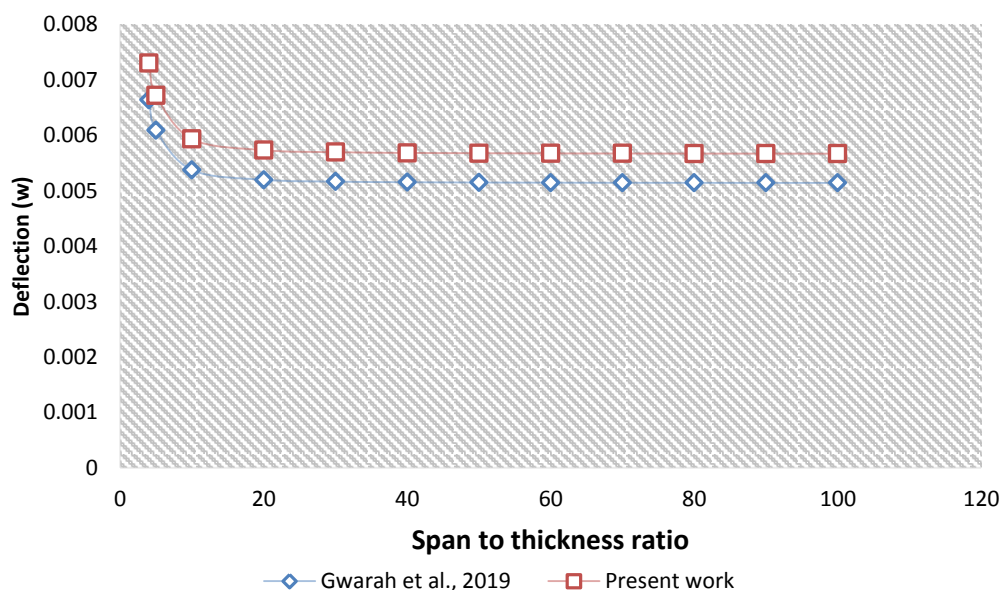


Figure 13: Plots of central deflection of CSFS square plate versus span-thickness ratio

## **7. Conclusion**

It is concluded that the values of critical lateral load obtained by this theory achieved accepted vertical shear stress to the thickness of plate variation and satisfied the transverse flexibility of the condition of the plate while predicting the bending behavior of an isotropic rectangular CSFS plate.

Furthermore, it can be concluded that the values of critical lateral load obtained by this theory achieve accepted vertical shear stress to the thickness of plate variation and satisfied the transverse flexibility of condition at the top and bottom faces of the plate while predicting the flexural characteristics for an isotropic rectangular CSFS plate. The deflection and stresses obtained by present theory are in good agreement with the other order theories. This validates the efficacy and credibility of the present polynomial shear deformation theory.

## **8. Recommendation**

This approach is recommended to the practicing engineers as it overcomes the challenges of the conventional practice in the structural analysis/design which involves checking of deflection and shear; the process which is proved unreliable.

## **References**

- Ghugal, YM. and Kulkarni, SK. 2011. Thermal stress analysis of cross-ply laminated plates using refined shear deformation theory. *Journal of Experimental and Applied Mechanics*, 2: 47-66.
- Ghugal, YM. and Sayyad, AS. 2011. Free vibration of thick isotropic plates using trigonometric shear deformation theory. *Journal of Solid Mechanics*, 3(2): 172-182.
- Ibearugbulem, OM. and Onyeka, FC. 2020. Moment and stress analysis solutions of clamped rectangular thick plate. *European Journal of Engineering Research and Science*, 5(4): 531-534.
- Gwarah, LS. 2019. Application of Shear Deformation Theory in the Analysis of Thick Rectangular Plates using Polynomial Displacement Functions. PhD. Thesis, Department of Civil Engineering, Federal University of Technology, Owerri, Nigeria.
- Mantari, AS., Oktem, C. and Guedes S. 2012. A new trigonometric shear deformation theory for isotropic, laminated composite and sandwich plates. *International Journal of Solids and Structures*, 49: 43-53.
- Mindlin, RD. 1951. Influence of rotary inertia and shear on flexural Motions of Isotropic, Elastic Plates. *ASME Journal Applied Mechanics*, 18: 31-38.
- Onyeka, FC. 2019. Direct analysis of critical lateral load in a thick rectangular plate using refined plate theory. *International Journal of Civil Engineering and Technology*, 10(5): 492-505.
- Onyeka, FC. and Ibearugbulem, OM. 2020. Load analysis and bending solutions of rectangular thick plate. *International Journal on Emerging Technologies*, 11(3): 1103-1110.
- Onyeka, FC., Okafor, FO. and Onah, HN. 2018. Displacement and stress analysis in shear deformable thick plate. *International Journal of Applied Engineering Research*, 13(11): 9893-9908.
- Onyeka, FC., Okeke TE. and Wasiu, J. 2020. Strain–displacement expressions and their effect on the deflection and strength of plate. *Advances in Science, Technology and Engineering Systems*, 5(5): 401-413.
- Pagano NJ. 1967. Exact solutions for composite laminates in cylindrical bending. *Journal of Composite Materials*, 3: 398-411.

Pipes RB. and Pagano NJ. 1970. Interlaminar stresses in composite laminates under axial extension. *Journal of Composite Materials*, 4: 538-648.

Reddy JN. 1984. A refined non-linear theory of plates with transverse shear deformation. *International Journal of Solids and Structures*, 20: 881-896.

Reissner, E. 1945. The effect of transverse shear deformations on the bending of elastic plates. *ASME Journal of Applied Mechanics*, 12: A69-A77.

Sayyad, AS. and Ghugal, YM. 2012a. Bending and free vibration analysis of thick isotropic plates by using exponential shear deformation theory. *Applied and Computational Mechanics*, 6(1): 65-82.

Sayyad, AS. and Ghugal, YM. 2012b. Buckling analysis of thick isotropic plates by using exponential shear deformation theory. *Applied and Computational Mechanics*, 6(2): 185-196.

Soldatos, KP. 1988. On certain refined theories for plate bending. *ASME Journal of Applied Mechanics*, 55: 994-995.

Soldatos, KP. 1992. A transverse shear deformation theory for homogeneous monoclinic plates. *Acta Mechanica*, 94: 195-200